Considine, J.M.; Pierron, F.; Turner, K.T.; Vahey, D.W. 2013. Anisotropy evaluation of paperboard with virtual fields method. In: Proceedings of 2013 SEM annual conference and exposition on experimental and applied mechanics. 2013 June 3-5; Lombard, IL. Paper 83.

Anisotropy Evaluation of Paperboard With Virtual Fields Method

J.M. Considine
Materials Research Engineer
US Forest Service, Forest Products Laboratory
One Gifford Pinchot Drive
Madison, WI, USA 53726

F. Pierron
Professor
University of Southampton
Southampton SO17 1BJ, UK

K.T. Turner
Associate Professor
University of Pennsylvania
245 Towne Building
220 S. 33rd St
Philadelphia, PA, USA, 19104-6315

D.W. Vahey
Materials Research Engineer
US Forest Service, Forest Products Laboratory
One Gifford Pinchot Drive
Madison, WI, USA 53726

ABSTRACT

Paperboard is most often used as a structural material in which stiffness is a critical mechanical property. As such, paperboard mills use stiffness as one of their quality control parameters. Some manufacturing variability of paperboard is caused by changing material anisotropy, a behavior that is difficult to characterize. This work introduces a novel load fixture, designed to produce full-field strains capable of anisotropic Q_{ij} evaluation without wrinkling the paperboard specimen. Anisotropic Q_{ij} evaluation was accomplished using the Virtual Fields Method (VFM), a generalized inverse method. A substantial effort was made to ensure material remained in its linear elastic regime. Q_{ij} determined by the VFM compared favorably with those determined by ultrasonic and tensile coupon tests. An appropriate virtual field mesh was established by a mesh density analysis.

Keywords: VFM, DIC, stiffness, paperboard, anisotropy

Introduction

Determination of mechanical properties of paper and paperboard is a critical part of quality control processes in paper mills because these properties largely regulate product value. Variability of mechanical properties is rarely acknowledged outside the industry [1]. One significant cause of variability is anisotropy. Anisotropy has many sources, some of which are fiber misalignment (i.e., predominant fiber direction is not aligned with direction of web travel), nonuniform drawing forces and uneven drying. As cellulose fiber materials are generally sold on a strength/weight or stiffness/weight basis, reduction of product variability and mechanical property improvement are persistent goals of paper manufacturers. Two tests, tensile coupon and ultrasonic, are the most common evaluations used for mechanical property determination; however, both have difficulty

assessing anisotropy. Whereas tensile testing is destructive and requires multiple specimens at several angles of orthotropy, ultrasonic testing requires independent measurement of Q_{66} or Q_{12} [2] and depends on relatively few degrees of freedom.

Some degree of anisotropy in cellulose fiber composites, such as paper and paperboard, is expected, because cellulose fibers are themselves anisotropic [3]. Macroscopically, anisotropy is influenced by fiber orientation distribution and drying stresses [4, 5]. Online stiffness measurement is used in process control [6] to reduce anisotropy.

Full-field measurement techniques, such as DIC (digital image correlation), combined with analysis techniques developed to use this spatially dense data, offer another method to assess material anisotropy. In particular, VFM (Virtual Fields Method) [7] provides a unique combination of speed, programming simplicity, and multiple parameter assessment from a single test. VFM has been successfully employed to determine anisotropic plate bending stiffnesses [8] and through-thickness rigidities of thick composite tubes [9].

The objective of this paper is to demonstrate the use of VFM with full-field DIC-measured strain data to determine the anisotropic stiffnesses of a paperboard material by use of a novel load fixture. Appropriateness of this approach is demonstrated by comparison with stiffness determined by the two commonly used methods, namely ultrasonic and tensile coupon tests, which assume material homogeneity.

Material

Material was Whatman® (Kent, U.K.) Chromatography Paper 3MM CHR, often called filter paper. It had nominal physical properties of grammage 180 gm/m^2, thickness 0.28 mm and density 635 kg/m^3. Although no exact definition exists for the term paperboard, this filter paper had a thickness generally associated with paperboards and will be referred to as paperboard or filter paper. Filter papers are used in a variety of household, commercial, and scientific applications to capture particulate matter. The material was 100% cellulose, composed entirely of cotton linters, a cellulose fiber that is typically 5-10 mm long. Paperboards are considered within the paper industry to be orthotropic. Paperboards contain variability from side-to-side of the web and along web length. Side-to-side variability is generally much greater than variability along web length. Paper machinery manufacturers have developed equipment to greatly reduce through-thickness variability.

Load Fixture

A specially designed load fixture is shown in Figure 1. External forces are applied through four grips on the top half of the fixture and measured with Sensotec (Honeywell International, Inc., Columbus, Ohio) Model 31BR load cells (range $\pm$444 N) attached to Sensotec Model GM signal conditioners. The four grips located on the bottom half of the specimen are stationary. Another fixture, not shown, was used to cut the specimen and properly locate and punch holes for each grip. Prior to placing the specimen within the fixture, an alignment jig was used to adjust the top four grips to a precise starting location such that the specimen would experience no forces upon initial placement in the fixture. The aluminum knobs shown in Figure 1b are rotated to generate a particular radial tensile force at that location. Multiple load configurations were used to create a series of different full-field strains for Q_{ij} evaluation. For each load configuration, individual forces were kept constant or increased, with respect to the previous load configuration, so that relaxation stiffnesses were avoided.

The 24.5-cm-diameter specimen was gripped at eight locations 45° apart. Grips consisted of two small brass plates approximately 12 mm square. One plate had a threaded hole; the other a through-hole. Holes were punched at grip locations in the specimen, which was then clamped between plates with a small bolt. A torque wrench was used to ensure uniform clamping pressure for each grip. Special care was taken to prevent the top brass gripping plate from twisting and introducing undesirable stresses on the specimen.

Digital Image Correlation

We examined the paperboard surface with a Dantec® (Dantec Dynamics, Inc., Holtsville, New York) DIC system whose details are listed in Table 1. Dot pattern was photocopied on specimens with a Sharp® (Sharp Electronics Corp., Mahwah, New Jersey) MX-3100N copier. Static specimen images were captured by waiting 5 min after load application was adjusted. A single reference image was used for each test. For each specimen, the first load configuration had forces approximately 15 N greater, at each load grip, than forces for the reference image. Forces on the specimen for the reference image were used to ensure that the specimen was planar.

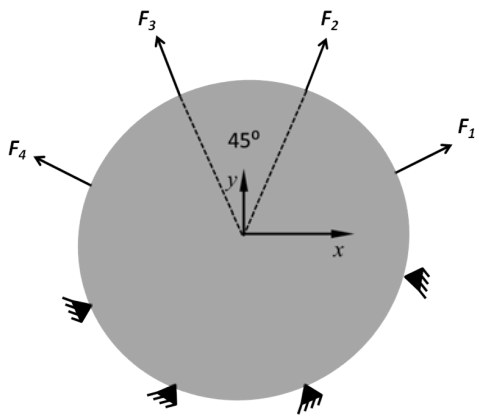

(a) Schematic of load fixture

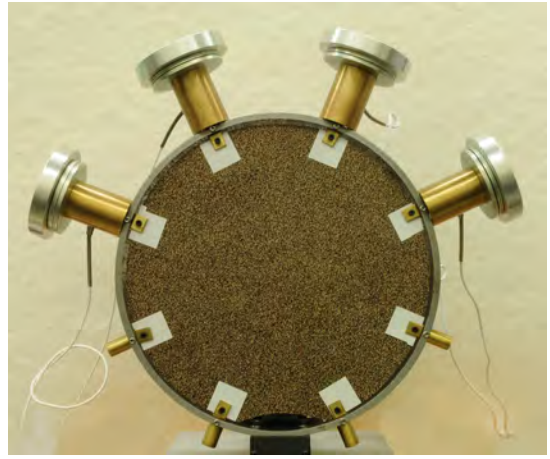

(b) Actual load fixture

Figure 1: Load Fixture

Technique Used	Stereo Image Correlation
Camera	Allied Vision Technologies (Stadtroda, Germany) Stingray Model F504B
Lens	Computar (Commack, NY) M1614-MP2, 16 mm, f1.4
Lighting	Red LED, 4x3 array, wavelength 610-640 nm
Interface	IEEE 1394b - 800 Mb/s
Resolution	2452 x 2056
Sensor	Sony (Sony America, New York, NY) ICX655, CCD Progressive
Sensor Size	Type 2/3
Lens Mount	C
Field of View	38.7 cm x 32 cm
Facet Size	21 pixels, approx 3.3 mm x 3.3 mm
Software	Istra (Dantec) 4-D v2.1.5
Smoothing	7x7 adaptive polynomial

Table 1: DIC system components and parameters

Virtual Fields Method

An abbreviated introduction to VFM is presented here; a recent book [7] provides a more thorough presentation. For a plane stress problem, the Principle of Virtual Work can be written as

$$\int_S (\sigma_1 \varepsilon_1^* + \sigma_2 \varepsilon_2^* + \sigma_6 \varepsilon_6^*)\, dS = \int_{L_f} \bar{T}_i u_i^* dl \tag{1}$$

where S is the area of 2-D domain, σ_i are stresses within S, u_i^* are kinematically admissible virtual displacements, ε_i^* are virtual strains associated with u_i^*, $\bar{T}_i$ are tractions applied on boundary of S, and L_f is the portion of S over which $\bar{T}_i$ are applied.

Assuming a linear elastic anisotropic material, the constitutive equation, using contracted index notation, is given by

$$\begin{Bmatrix} \sigma_1 \\ \sigma_2 \\ \sigma_6 \end{Bmatrix} = \begin{bmatrix} Q_{11} & Q_{12} & Q_{16} \\ Q_{12} & Q_{22} & Q_{23} \\ Q_{16} & Q_{26} & Q_{66} \end{bmatrix} \begin{Bmatrix} \varepsilon_1 \\ \varepsilon_2 \\ \varepsilon_6 \end{Bmatrix} \tag{2}$$

Substituting Equation 2 into Equation 1 gives

$$\begin{aligned} &\int_S Q_{11} \varepsilon_1 \varepsilon_1^* + \int_S Q_{22} \varepsilon_2 \varepsilon_2^* dS + \int_S Q_{12} (\varepsilon_1 \varepsilon_2^* + \varepsilon_2 \varepsilon_1^*)\, dS + \cdots \\ &\cdots + \int_S Q_{16} (\varepsilon_1 \varepsilon_6^* + \varepsilon_6 \varepsilon_1^*)\, dS + \int_S Q_{26} (\varepsilon_2 \varepsilon_6^* + \varepsilon_2 \varepsilon_6^*)\, dS + \int_S Q_{66} \varepsilon_6 \varepsilon_6^* dS = \int_{L_f} \bar{T}_i u_i^* dl \end{aligned} \tag{3}$$

If the material is homogeneous, then each Q_{ij} is a constant and can be placed outside the integrals in Equation 3. In practice, six different u_i^* are used in Equation 3, one to identify each Q_{ij}. Special virtual fields simplify identification by choosing a u_i^* so that only one integral term exists on the left side of Equation 3. By approximating the integrals in Equation 3 as discrete summations, a system of linear equations is developed whose solution requires minimal computation. DIC provides information on each ε_i throughout specimen surface and load cells provide values for each $\bar{T}_i$.

One of the most direct methods to create the virtual fields is to define a mesh of 4-node quadrilateral isoparametric elements, as shown in Figure 2. In order to have a kinematically admissible virtual field, grip nodes are virtually fixed in both u and v displacement because they correspond to stationary grips in Figure 1a. Additionally, load grips are restricted to radial displacement corresponding to forces F_4, F_3, F_2 and F_1. VFM elements in Figure 2 are not precisely rectangular as some asymmetry of grip and force locations was created during fabrication. VFM meshes are not required to conform to specimen boundaries. Some VFM elements lie completely outside the specimen area, S, while other elements straddle the external boundary of S. Only terms in Equation 3 with nonzero, experimentally-measured ε_i have a contribution to stiffness evaluation.

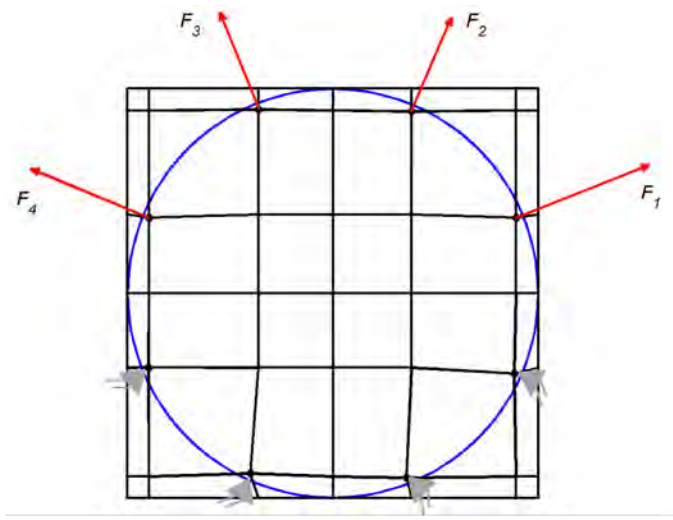

Figure 2: Example of 36-element virtual mesh for Figure 1a

Supporting Tests

Ultrasonic tests were performed with a Nomura Shoji® (Tokyo, Japan) SST-250 paper tester. Transmission probe oscillated at 25 kHz. A central circular region of 15-cm diameter was examined for each specimen. Ultrasonic velocity was measured from 0° to 175° in 5° increments. Q_{66} was determined by measuring shear wave velocity transmitted along the 2-principal material direction using a second, modified SST instrument. Remaining stiffnesses were determined by nonlinear regression of the stiffness transformation matrix [10].

Three tensile coupons were cut from each circular specimen after DIC and ultrasonic evaluations. Coupons were cut at 0°, 45°, 90° from 1-principal material direction. Coupons were 25 mm wide and each had a nominal gage length of 175 mm. Specimens were tested in an Instron® (Instron Corp., Norwood, Massachusetts) Model 5865 load frame with a grip displacement rate of 0.5 mm/min. DIC images were captured at 1 Hz and used to determine longitudinal and transverse strains. Longitudinal strains were used to determine Q_{11} and Q_{22}; transverse strains were used to determine ν_{12}; Q_{66} was determined by stiffness transformation.

Results and Discussion

Table 2 gives VFM-evaluated Q_{ij} for the first and second tests of the same specimen, where tests are noted in column 1. Units are km^2/s^2, or specific stiffness units, and are equivalent to MN · m/kg. To minimize effects of relaxation on measurement, each subsequent load configuration had each of its forces held constant or increased from previous load configuration. After the first test, the specimen was removed from the load fixture, grips were reset to their initial locations, the specimen was re-installed in the fixture, and forces were introduced. Test 2 had small decreases in F_1 and F_4; however, it appears that corresponding large increases in F_2 and F_3 avoided relaxation of the material.

Table 2: Q_{ij} evaluation for each test of the specimen using mesh in Figure 2. Stiffness units (km^2/s^2), Force units (N). LC - load configuration

Test	LC	Q_{11}	Q_{22}	Q_{12}	Q_{66}	Q_{16}	Q_{26}	F_1	F_2	F_3	F_4
1	1	2.87	6.81	0.61	1.29	-0.12	0.06	16.9	17.3	19.0	17.8
	2	2.87	6.96	0.62	1.36	-0.08	-0.25	18.2	21.4	27.5	19.1
	3	2.61	6.12	0.75	1.37	-0.06	-0.42	19.1	22.7	27.6	20.9
	4	2.62	6.09	0.68	1.16	-0.05	-0.21	21.8	26.7	29.5	22.2
	5	2.59	5.86	0.72	1.26	0.00	-0.33	24.0	30.7	32.7	25.4
	6	2.65	5.98	0.73	1.29	0.02	-0.60	25.8	35.6	38.5	30.7
	7	2.52	5.90	0.71	1.21	0.05	-0.58	28.5	37.4	39.1	32.0
	8	2.45	5.53	0.58	1.17	0.07	-0.57	29.8	38.3	40.0	33.4
	9	2.35	5.55	0.63	1.16	0.06	-0.61	33.4	42.3	45.3	37.4
	10	2.28	5.44	0.60	1.14	0.06	-0.67	35.1	44.0	47.5	40.0
	mean	2.58	6.02	0.66	1.24	-0.01	-0.42				
	COV (%)	7.49	8.50	9.60	6.89	-1264.91	-55.48				
2	1	3.65	6.72	0.56	1.74	-0.08	0.13	17.8	16.0	17.9	15.6
	2	3.25	6.66	0.58	1.63	-0.10	0.35	17.3	20.0	21.3	14.7
	3	3.00	6.88	0.23	1.61	-0.31	0.37	18.2	22.7	24.3	17.3
	4	2.95	6.68	0.47	1.55	-0.07	0.07	20.5	26.7	27.8	20.0
	5	2.91	6.56	0.56	1.44	0.00	0.03	23.1	28.9	29.7	21.8
	6	2.83	6.05	0.31	1.29	0.03	0.17	25.4	30.7	31.4	21.8
	7	3.00	6.26	0.26	1.20	0.09	0.07	26.7	34.7	35.8	23.6
	8	2.93	6.02	0.27	1.22	0.09	0.12	29.4	36.5	37.9	25.4
	9	2.81	6.11	0.22	1.17	-0.00	0.13	32.0	38.3	41.5	28.5
	10	2.72	6.08	0.34	1.17	0.00	0.18	36.9	44.0	44.3	33.8
	mean	3.01	6.40	0.38	1.40	-0.04	0.16				
	COV (%)	8.90	5.19	38.18	15.61	-331.35	69.44				

Results shown in Table 2 indicate the specimen was generally oriented with its primary principal material direction aligned vertically, because Q_{22} was greater than Q_{11}. Each test had reasonable agreement for Q_{11}, Q_{22}, Q_{12}, and Q_{66}, as demonstrated by acceptable COVs (coefficients of variation). COVs were generally below 10% for the largest Q_{ij}. In both tests, increases in applied forces tended to give reduced Q_{ij}.

Amount of anisotropy, as indicated by non-zero Q_{16} and Q_{26}, was quite small. Habeger [2] suggested that anisotropy can be characterized by comparing non-orthogonality of directions for maximums of Q_{11} and Q_{22}. Using the mean values for Q_{ij} from Table 2 Test 1, 1- and 2-directions differ by 90.1°. Using mean values for the second test, 1- and 2-directions differ by 89.7°. Because the non-orthogonality was quite small, the specimen was considered orthotropic. One encouraging result was the generally consistent opposing signs for Q_{16} and Q_{26}, which is a necessary result from stiffness transformation of orthotropic materials.

Q_{11}, Q_{22}, Q_{12}, and Q_{66} decreased with increasing applied forces. This trend is shown graphically in Figure 3, where "norm" refers to 2-norm for applied force and stiffness. The largest stiffness values, Q_{11}, Q_{22}, and Q_{66}, largely control the 2-norm. Because the evaluation procedure described here determined secant Q_{ij} and the selected material was known to be nonlinear, additional analyses were made to examine the possiblity that the load configurations may have taken the material into nonlinear constitutive behavior.

Determination of material nonlinear behavior is not straightforward for this load fixture. Because the geometry was intentionally designed to produce sufficient strains, ε_i, for evaluation of all six Q_{ij}, it is not possible to directly determine onset of material nonlinear behavior. Furthermore, nonlinear behavior is unlikely to occur simultaneously for each Q_{ij}. Figure 4 examines the manner in which forces induced strain in these tests. This figure suggests that the specimen behaved linear elastically for each load configuration and for each test. Elastic behavior is illustrated by the relative coincidence of points for each test.

Table 3 compares Q_{ij} for VFM, ultrasonic, and tensile coupon tests. Both ultrasonic and tensile tests assume linear constitutive behavior. All three tests have reasonable agreement for Q_{11}, Q_{22}, and Q_{66}, which provides further evidence that the

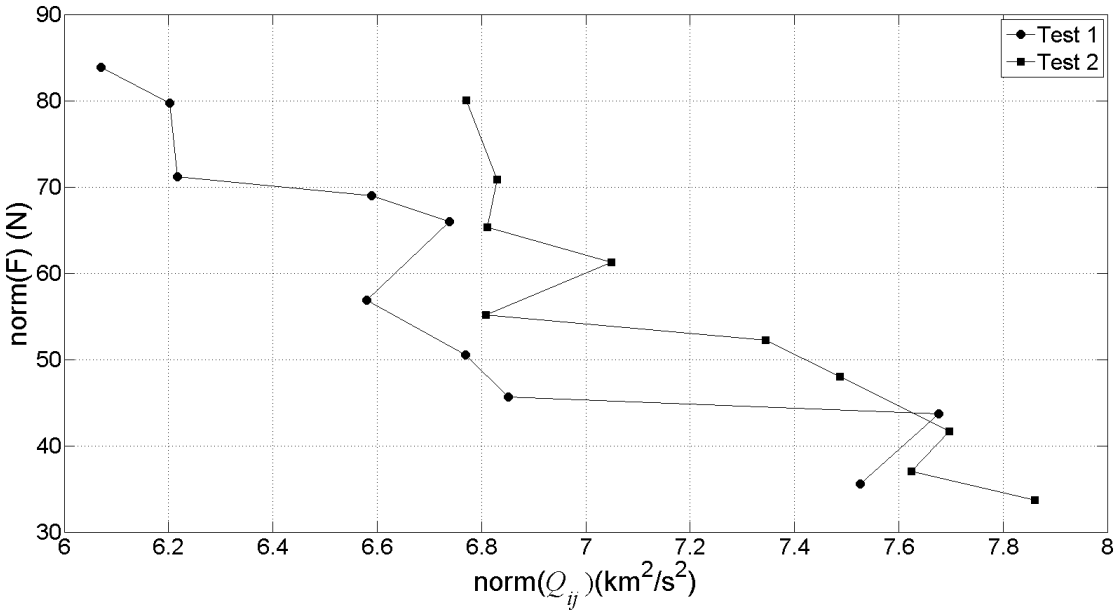

Figure 3: Normalized stiffness, Q_{ij}, as affected by normalized applied force, F_i

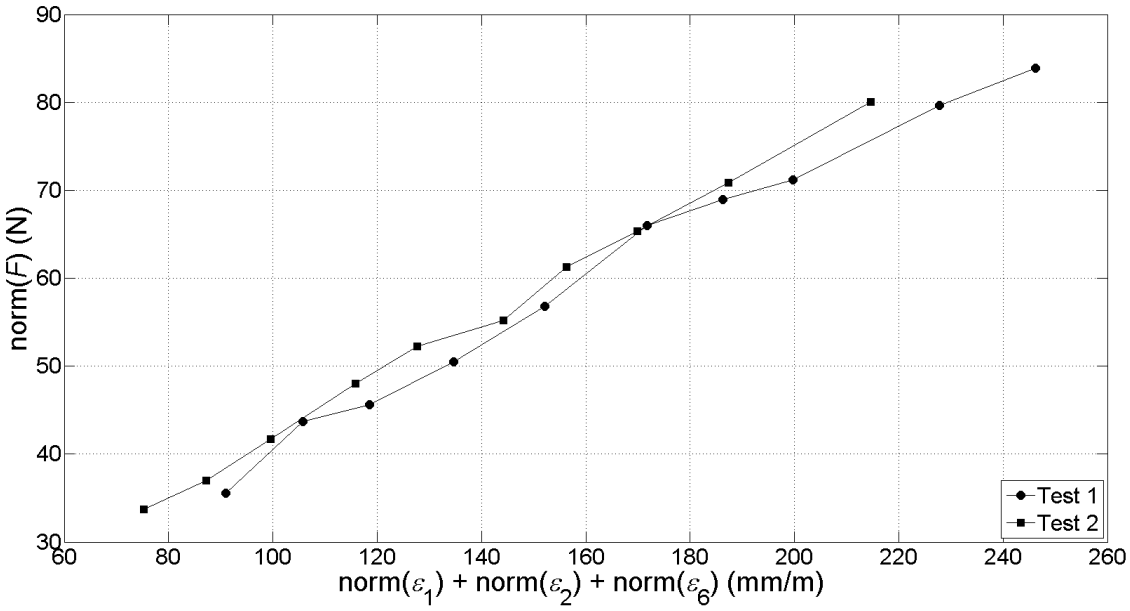

Figure 4: Examination of applied forces and induced strain for Tests 1 and 2

various load configurations in Tests 1 and 2 were within the linear material regime. VFM-evaluated Q_{12} were much smaller than ultrasonic and tensile Q_{12}. Ultrasonic evaluation of Q_{12} is difficult and generally produces high values [11]. Additionally, Q_{66} and Q_{12} are effectively coupled in ultrasonic measurements because Q_{ij} are evaluated by stiffness matrix transformation. VFM-evaluated ν_{12} were 0.11 and 0.06 for Test 1 and Test 2 respectively, which falls below the range of ultrasonic ν_{12} values reported by Baum et al. [12]. Alternative explanations for Q_{12} disagreement between tests include number of Q_{ij} evaluations and specimen area examined for each test. VFM evaluation was based on the mean of 10 Q_{ij} identifications; ultrasonic values were based on a single test; three tensile coupons were evaluated, but Q_{12} was based on measurements made on two of those tensile coupons. If heterogeneity existed in the specimen, then relative area tested for each test would influence identification. Test areas were 471, 177, and 131 cm^2 for VFM, ultrasonic, and tensile tests, respectively.

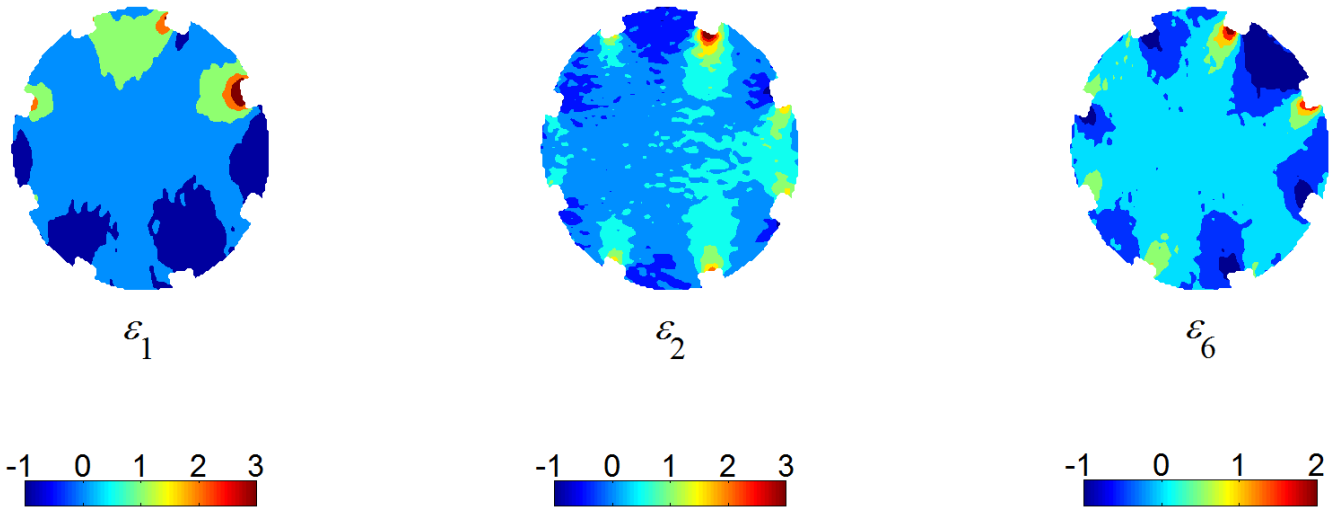

Figure 5: Strains for Test 1, Load Configuration 10, Units (mm/m)

To determine Q_{66}, significant effort was made to generate shear strains by creating a large force differential between adjacent loading grips. Figure 5 shows DIC-measured strains for Test 1, Load Configuation 10 where F_1-F_4 were 36.9, 44.0, 44.3, and 33.8 N, respectively. For this configuration, ε_6 was near zero throughout the central region of the specimen. However, if the force differential became too large, the specimen developed wrinkles and the test was terminated. It is likely that some prior knowledge of approximate Q_{ij} may be used to create a specific load configuration optimized for stiffness evaluation. Accurate determination of Q_{66} for thin webs is a challenge and successful Q_{66} evaluation here demonstrates an alternative procedure, on a single specimen, without difficulties associated with ultrasonic and tensile tests.

VFM and ultrasonic tests had general agreement for both Q_{16} and Q_{26}. When Q_{16} and Q_{26} are very near zero, their evaluation tends to get masked by larger Q_{ij} for both VFM and ultrasonic tests. Ultrasonic test gave an angle of 90.1° between material 1- and 2-directions.

Table 3: Comparison of different methods for evaluating Q_{ij}, Units km^2/s^2

Test	Q_{11}	Q_{22}	Q_{12}	Q_{66}	Q_{16}	Q_{26}
VFM-Test1	2.58	6.02	0.66	1.24	-0.01	-0.42
VFM-Test2	3.01	6.40	0.38	1.40	-0.04	0.16
Ultrasonic	3.33	7.12	1.94	1.68	0.12	-0.14
Tensile	2.80	6.22	1.29	1.42	N/A	N/A

Figure 6 examines the influence of VFM element density on Q_{ij} evaluation. Unlike finite element convergence analyses, increased VFM element density does not improve accuracy of Q_{ij} identification, but tends to amplify noise present in experimentally measured strains. A very coarse mesh (i.e., 5^2 elements) smoothed strain gradients, which were real features that were intentionally introduced in the load fixture. Reduction of norm(Q_{ij}) above 15^2 elements was caused by increasingly ill-conditioned matrices used to evaluate virtual displacements, u_i^*, in Equation 3.

Conclusion

This work introduced a novel load fixture designed to determine the anisotropic stiffnesses of paperboard with VFM. DIC was used to determine full-field strains under a variety of multi-axial load configurations. Because paperboard is considered to have nonlinear constitutive behavior, special analyses were introduced to examine material nonlinearity and elasticity. Analyses demonstrated that the material remained in the linear elastic regime because VFM-evaluated Q_{ij} were repeatable and compared favorably with those determined by ultrasonic and tensile coupon tests. Finally, the effect of VFM mesh density was examined to ensure that an appropriately sized mesh was used in the analysis.

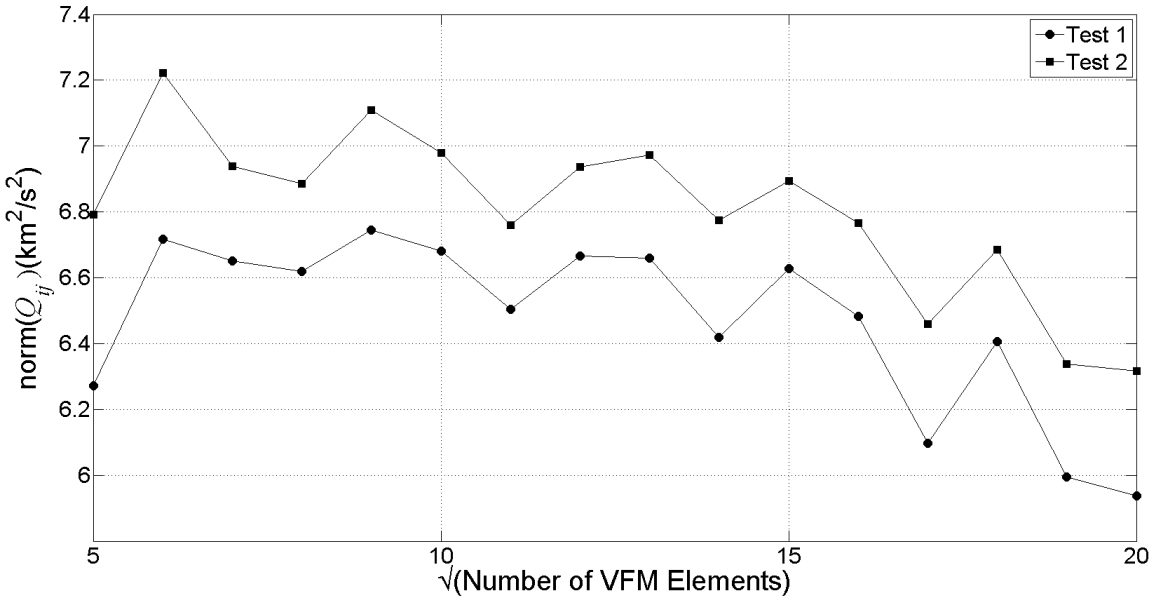

Figure 6: Effect of mesh density on Q_{ij} evaluation

References

[1] R. Allan, "The cost of paper property variation is high," *Appita*, vol. 65, no. 4, pp. 308–312, 2012.

[2] C. C. Habeger, "An ultrasonic technique for testing the orthotropic symmetry of polymeric sheets by measuring their elastic shear coupling-coefficients," *Journal of Engineering Materials and Technology-Transactions of the ASME*, vol. 112, no. 3, pp. 366–371, 1990.

[3] I. Diddens, B. Murphy, M. Krisch, and M. Muller, "Anisotropic elastic properties of cellulose measured using inelastic x-ray scattering," *Macromolecules*, vol. 41, no. 24, pp. 9755–9759, 2008.

[4] M. Htun, H. Andersson, and M. Rigdahl, "The influence of drying strategies on the anisotropy of paper in terms of network mechanics," *Fibre Science and Technology*, vol. 20, no. 3, pp. 165–175, 1984.

[5] G. L. Batten and A. H. Nissan, "Invariants in paper physics," *Tappi Journal*, vol. 69, no. 10, pp. 130–131, 1986.

[6] G. Baum, "Elastic properties, paper quality, and process control," *Appita*, vol. 40, no. 4, pp. 289–294, 1987.

[7] F. Pierron and M. Grédiac, *The Virtual Fields Method: Extracting Constitutive Mechanical Parameters from Full-Field Deformation Measurements*. Springer, 2012.

[8] M. Grédiac and A. Vautrin, "A new method for determination of bending rigidities of thin anisotropic plates," *Journal of Applied Mechanics-Transactions of the ASME*, vol. 57, no. 4, pp. 964–968, 1990.

[9] R. Moulart, S. Avril, and F. Pierron, "Identification of the through-thickness rigidities of a thick laminated composite tube," *Composites Part A-Applied Science and Manufacturing*, vol. 37, no. 2, pp. 326–336, 2006.

[10] R. Jones, *Mechanics of Composite Materials*. Taylor & Francis London, 1975.

[11] T. Uesaka, K. Mukarami, and R. Imamura, "On the poisson's ratio of paper and its experimental determination," *Tappi*, vol. 65, no. 8, pp. 115–116, 1982.

[12] G. Baum, D. Brennan, and C. Habeger, "Orthotropic elastic constants of paper," *Tappi Journal*, vol. 64, no. 8, pp. 97–101, 1981.